drones

MDPI

Article

Dual-UAV Collaborative High-Precision Passive Localization Method Based on Optoelectronic Platform

Xu Kang [1,2], Yu Shao [1,2], Guanbing Bai [1], He Sun [1], Tao Zhang [1,2] and Dejiang Wang [1,*]

[1] Key Laboratory of Airborne Optical Imaging and Measurement, Changchun Institute of Optics Fine Mechanics and Physics Chinese Academy of Sciences, Changchun 130033, China; xkang2019@163.com (X.K.); shaoy4158@gmail.com (Y.S.); 17743017276@163.com (G.B.); sunhe_ciomp@163.com (H.S.); zhangt@ciomp.ac.cn (T.Z.)

[2] School of Optoelectronics, University of the Chinese Academy of Sciences, Beijing 101408, China

* Correspondence: wangdj04@ciomp.ac.cn

Abstract: Utilizing the optical characteristics of the target for detection and localization does not require actively emitting signals and has the advantage of strong concealment. Once the optoelectronic platform mounted on the unmanned aerial vehicle (UAV) detects the target, the vector pointing to the target in the camera coordinate system can estimate the angle of arrival (AOA) of the target relative to the UAV in the Earth-centered Earth-fixed (ECEF) coordinate system through a series of rotation transformations. By employing two UAVs and the corresponding AOA measurements, passive localization of an unknown target is possible. To achieve high-precision target localization, this paper investigates the following three aspects. Firstly, two error transfer models are established to estimate the noise distributions of the AOA and the UAV position in the ECEF coordinate system. Next, to reduce estimation errors, a weighted least squares (WLS) estimator is designed. Theoretical analysis proves that the mean squared error (MSE) of the target position estimation can reach the Cramér–Rao lower bound (CRLB) under the condition of small noise. Finally, we study the optimal placement problem of two coplanar UAVs relative to the target based on the D-optimality criterion and provide explicit conclusions. Simulation experiments validate the effectiveness of the localization method.

Keywords: optoelectronic platform; UAVs; AOA; CRLB; D-optimality criterion; optimal placement

Citation: Kang, X.; Shao, Y.; Bai, G.; Sun, H.; Zhang, T.; Wang, D. Dual-UAV Collaborative High-Precision Passive Localization Method Based on Optoelectronic Platform. *Drones* **2023**, *7*, 646. https://doi.org/10.3390/drones7110646

Academic Editors: Xiaoguang Liu, Dashuai Wang and Sheng Xu

Received: 26 August 2023
Revised: 27 September 2023
Accepted: 30 September 2023
Published: 25 October 2023

1. Introduction

Localization refers to the process of estimating the spatial position of a target using measurements obtained from the target. It is widely applied in the military and civilian fields [1–6]. Commonly used measurements in the localization process include time difference of arrival (TDOA) [7], time of arrival (TOA) [8], received signal strength (RSS) [9], angle of arrival (AOA) [4,10], and their combinations [11]. Among them, in addition to radio signals, compared with TDOA, AOA can also utilize the optical signal reflected by the target for observation. Therefore, the localization based on TDOA and AOA does not require the unmanned aerial vehicle (UAV) to actively emit signals. Instead, it estimates the position of an unknown target solely by receiving signals relevant to the target in the surrounding environment, thus providing stronger concealment.

Compared to TOA, TDOA does not require strict time synchronization but still requires additional transmitters [12]. Kim et al. estimated that the AOA of a target using antenna arrays also necessitates signal transmitters [13]. In both scenarios, UAVs can achieve passive target localization, but they introduce exposure risks to the transmitters. However, optoelectronic platforms can detect visible light reflected by the target or infrared radiation from the target itself. Through signal processing, target detection, tracking, and a series of coordinate transformations, the optoelectronic platform obtains the line-of-sight (LOS) vector pointing to the target [14], and the AOA of the target can be obtained through simple algebraic calculations. Therefore, estimating AOA based on the optical characteristics

possesses inherent advantages in terms of concealment. When localizing targets in three-dimensional (3D) space, TDOA requires at least four observation stations, while two UAVs equipped with optoelectronic platforms can covertly detect and locate targets.

After the optoelectronic platform detects the target, a series of coordinate transformations and algebraic calculations are involved in the process from the LOS vector to estimate the AOA of the target. The parameters used in each calculation process are subject to noise interference, which collectively affects the estimation error of AOA. The UAV obtains its longitude, latitude, and altitude in the World Geodetic System 1984 (WGS84) coordinate system through the global positioning system (GPS), while the position estimation of the target is realized in the Earth-centered Earth-fixed (ECEF) coordinate system. In addition to AOA, it is also necessary to estimate the UAV position in the ECEF coordinate system and its noise distribution. All these factors ultimately affect the accuracy of target localization.

AOA refers to azimuth in a two-dimensional (2D) plane and represents both azimuth and elevation in 3D space. The relationship between AOA and the target position is nonlinear, making direct solutions challenging. Maximum likelihood estimation (MLE) offers asymptotically unbiased localization performance and is a commonly used method for solving nonlinear problems. However, MLE requires iterative computations and demands high precision in the initial values. Numerous studies have proposed various localization methods [15–18] by utilizing known UAV positions, AOA measurements, and their noise distributions. In [15], the problem of bias in MLE is analyzed in detail. In [16,17], they employed a semi-definite relaxation (SDR) approach to unify near-field and far-field localization using modified polar coordinate representation. Subsequently, [18] proposed an algebraic solution for modified polar coordinate representation. In [10], the bias compensation problem of pseudo-linear localization algorithms was investigated. In [4], the position error of the observation station was considered, and an asymptotically unbiased closed-form solution for target localization was proposed. The mean squared error (MSE) of target position estimation can achieve the Cramér–Rao lower bound (CRLB). When localizing targets using UAVs equipped with optoelectronic platforms, both measurement errors and the position errors of the UAV exist simultaneously. This paper presents a weighted least squares (WLS) algorithm, and theoretical analysis demonstrates that its estimation accuracy can achieve the CRLB under small error conditions.

The different localization algorithms aim to improve the estimation accuracy of the target position in a given positioning scenario, but the performance of the algorithms has an upper limit. The CRLB is commonly employed to evaluate the localization performance of the algorithms. The geometric layout between the target and the UAV determines the upper limit of the localization accuracy. Optimizing the layout between the target and the UAV is an effective method to achieve high-precision positioning. When the noise obeys Gaussian distribution, the CRLB is equivalent to the inverse of the Fisher information matrix (FIM). Currently, three commonly used geometric configuration optimization criteria based on the CRLB and FIM have been proposed: A-, D-, and E-optimality criteria. Their physical meanings are, respectively, to minimize the sum of the three semi-major axes of the error ellipsoid, minimize the volume of the error ellipsoid, and minimize the maximum semi-major axis of the error ellipsoid. There is no superiority or inferiority among these three optimal optimization criteria, and the appropriate optimality criterion should be chosen based on specific usage scenarios.

In-depth research has been conducted on different localization scenarios based on these three optimality criteria. In the 2D plane, the objective functions of the three optimality criteria are equivalent in distance-based positioning scenarios [19]. Under the assumption of equal distances between the target and the observation stations, the D-optimality criterion has been used to investigate the optimal layout problem for bearing-only positioning [20]. When the positions of the observation stations are constrained in the 2D plane, this means that the optimal layout of a finite number of observation stations relative to the target has been studied [21]. In [22], the A-optimality criterion was employed to investigate the optimal placement for AOA-based positioning in unconstrained conditions in 3D space.

The flight altitude of UAVs is generally consistent during collaborative mission execution. To ensure the concealment of UAVs, maintaining a certain distance from the target is required when performing passive target localization. At this point, the layout of the target relative to the UAVs is constrained, and the conclusions from existing research cannot be effectively applied. The D-optimality criterion, which minimizes the volume of the error ellipsoid, provides an intuitive optimization direction. In this paper, we investigate the optimal layout of coplanar UAVs relative to the target based on the D-optimality criterion.

In summary, we have proposed a scheme for achieving high-precision passive localization of targets through the collaboration of two UAVs equipped with optoelectronic platforms. This paper presents three main research aspects as follows:

- Two noise transfer models are established to obtain the noise distributions of the UAV position and the AOA of the target relative to the UAV in the ECEF coordinate system;
- A WLS algorithm is proposed, taking into account the noise distributions of both the UAV position and the AOA;
- The optimal placement for two coplanar UAVs relative to the target is investigated using the D-optimality criterion, based on the FIM obtained from 3D space AOA measurements.

The remaining sections of this paper are outlined as follows: Section 2 focuses on estimating the AOA of the target and UAV position within the ECEF coordinate system, including their associated noise distributions. In Section 3, a weighted least squares estimator is proposed that takes into account both the UAV position error and AOA measurement error, and its theoretical localization performance is analyzed. Section 4 explores the optimal layout for coplanar dual UAVs relative to the target in 3D space, presenting an explicit solution. Section 5 validates the research conclusions through numerical simulation experiments. Section 6 summarizes this paper.

2. Estimation of Measurements and Their Error Distributions

The preconditions for utilizing the optoelectronic platform to localize targets are the known position of the UAV and the estimated AOA of the target relative to the UAV. This section firstly estimates the AOA of the target and its noise distribution based on the LOS vector. Then, the conversion relationship between the WGS84 coordinate system and the ECEF coordinate system is employed to estimate the position of the UAV and its noise distribution.

2.1. AOA of the Target Relative to UAV in the ECEF Coordinate System

Firstly, the coordinate system used in the process of estimating the LOS vector in the ECEF coordinate system by using the optoelectronic platform is introduced.

The ECEF coordinate system $(O_E - X_E Y_E Z_E)$ has the centroid of the Earth as its origin. The X_E axis points to the intersection of the prime meridian and the equator, the Z_E axis points to the North Pole, and the Y_E axes form a right-handed coordinate system with them. The geographic coordinate system $(O_G - X_G Y_G Z_G)$ selects the Local Cartesian coordinates (ENU) coordinate system as the geographic coordinate system. The origin is the centroid of the drone, and the X_G, Y_G, and Z_G axes point to east, north and up respectively. The UAV coordinate system $(O_U - X_U Y_U Z_U)$ takes the centroid of the UAV as the origin. X_U points to the nose of the UAV, and Z_U points to the top of the UAV. Y_U, X_U, and Z_U form a right-handed coordinate system. The base coordinate system $(O_B - X_B Y_B Z_B)$ takes the centroid of the optoelectronic platform frame as the origin, and the definition of the three axes is consistent with the UAV coordinate system. The camera coordinate system $(O_C - X_C Y_C Z_C)$ sets the camera centroid as the origin. In the initial state, the optical axis of the camera is Z_C pointing to the nose of the UAV, and X_C is vertical to the UAV. Y_C determines the orientation through the right-handed coordinate system. In the localization process, the distance between the target and the UAV is very great, and it can be approximated as particles. The origin of these coordinate systems on the UAV is approximately represented by the centroid of the UAV.

The procedure of determining the LOS vector in the ECEF coordinate system by the UAV through the optoelectronic platform is as follows: the camera searches the target area and moves it to the center of the field of view after detecting the target. There is an error when the target moves to the center of the image plane: the missing distance (x, y). Combined with the known focal length of the camera $f = 1.5$ m, the LOS vector $[x, y, f]^T$ in the camera coordinate system is obtained. The rotation of the camera in the base coordinate system when searching for the target is represented by the azimuth and elevation, (α, β). The base and the UAV are connected by shock absorbers, and the three vibration angles during the flight of the UAV are expressed as $(\varepsilon, \chi, \phi)$. At the same time, the flying attitude of the UAV also affects the LOS, and the attitude angle is (η, γ, κ). The position of of the UAV output by GPS in the WGS84 coordinate system is (L, M, H). The photoelectric platform can realize the relative angle measurement of the optical axis pointing and platform position isolated from an external disturbance in the inertial state. The measurement accuracy of these parameters determines the AOA estimation accuracy of the target relative to the UAV.

The translation operation between different coordinate systems will not affect the pointing of the LOS. The LOS vector in the camera coordinate system can be rotated multiple times to obtain the vector of the UAV pointing to the target in the ECEF coordinate system. The definitions of coordinate systems and parameters are shown in Figure 1. The meanings of these parameters and their corresponding error distributions are described in Table 1.

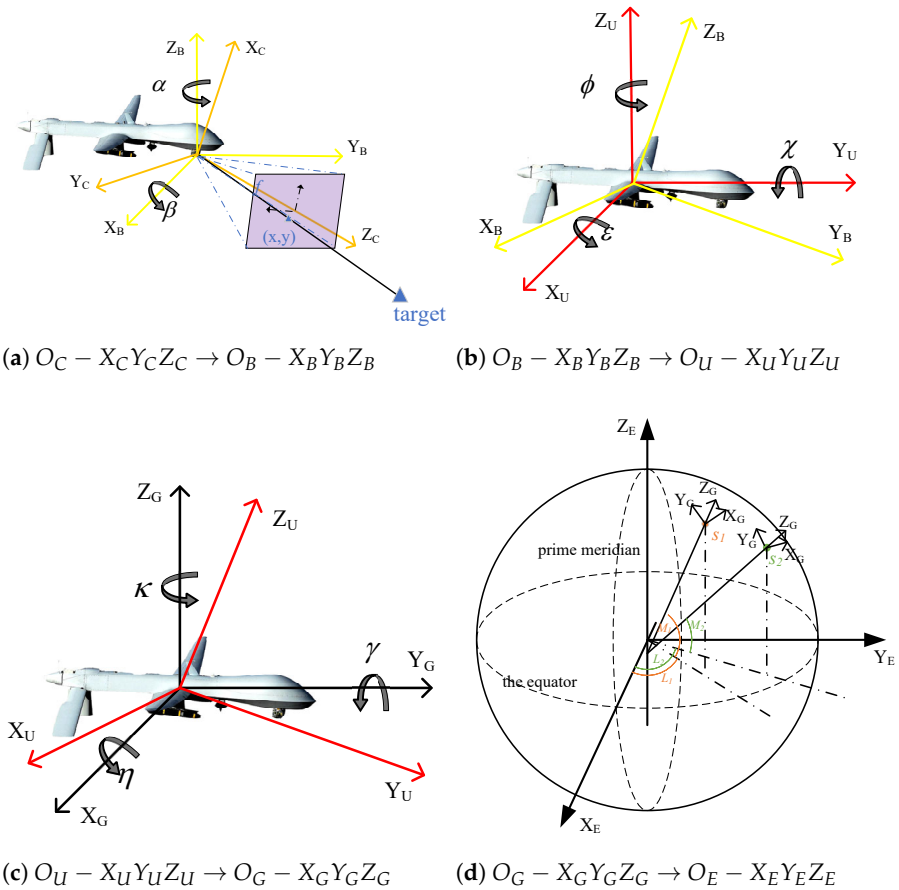

(**a**) $O_C - X_C Y_C Z_C \rightarrow O_B - X_B Y_B Z_B$ (**b**) $O_B - X_B Y_B Z_B \rightarrow O_U - X_U Y_U Z_U$

(**c**) $O_U - X_U Y_U Z_U \rightarrow O_G - X_G Y_G Z_G$ (**d**) $O_G - X_G Y_G Z_G \rightarrow O_E - X_E Y_E Z_E$

Figure 1. Several rotation transformations.

Table 1. Parameters used in estimating the AOA of the target and their error distribution.

Source of Error	Parameter	Random Distribution	Mean	Standard Deviation
Missing distance	x	Gaussian distribution	0	10 µm
	y	Gaussian distribution	0	10 µm
Gimbal angle	α (Azimuth)	Uniform distribution	0	0.01°
	β (Elevation)	Uniform distribution	0	0.01°
Vibration angle	ϕ (Heading)	Uniform distribution	0	0.01°
	χ (Pitch)	Uniform distribution	0	0.01°
	ε (Yaw)	Uniform distribution	0	0.01°
Attitude of UAV	κ (Heading)	Gaussian distribution	0	0.01°
	γ (Pitch)	Gaussian distribution	0	0.01°
	η (Yaw)	Gaussian distribution	0	0.05°
GPS of UAV	L (Longitude)	Gaussian distribution	0	0.0001°
	M (Latitude)	Gaussian distribution	0	0.0001°
	H (Height)	Gaussian distribution	0	10 m

The ECEF coordinate system is et as the final coordinate system for positioning the target. The LOS vector is expressed in the form of homogeneous coordinates as $[x/l\ , y/l\ , f/l\ ;, 1]^T$, where $l = \sqrt{x^2 + y^2 + f^2}$. When the measurements are disturbed by noise, these measurements are used to represent the true value through the Taylor formula.

If only the first-order noise is considered and the higher-order noise term is ignored, the modified Taylor formula is expressed as:

$$\begin{aligned} f(x) &= f(\tilde{x}) - f'(x)(\tilde{x} - x) \\ &= f(\tilde{x}) - f'(x)\Delta x \end{aligned} \tag{1}$$

Similarly, using the missing distance $\tilde{x}$ and $\tilde{y}$ interfered with by noise to represent the real LOS vector:

$$\begin{aligned} \mathbf{v}_{C,i} =& \left[x/l, y/l, f/l, 1\right]^T \\ =& \left[\tilde{x}/\tilde{l}, \tilde{y}/\tilde{l}, f/\tilde{l}, 1\right]^T - \mathbf{C}[\Delta x, \Delta y]^T \\ =& \tilde{\mathbf{v}}_{C,i} - \Delta\tilde{\mathbf{v}}_{C,i} \end{aligned} \tag{2}$$

where $\tilde{l} = \sqrt{\tilde{x}^2 + \tilde{y}^2 + f^2}$, $\mathbf{C} = \begin{bmatrix} \frac{\tilde{l}^2 - \tilde{x}^2}{\tilde{l}^3} & \frac{-\tilde{x}\tilde{y}}{\tilde{l}^3} & \frac{-\tilde{x}f}{\tilde{l}^3} & 0 \\ \frac{-\tilde{x}\tilde{y}}{\tilde{l}^3} & \frac{l^2 - \tilde{y}^2}{\tilde{l}^3} & \frac{-\tilde{y}f}{\tilde{l}^3} & 0 \end{bmatrix}^T$ is the Jacobian matrix of the LOS vector with respect to the missing distance.

The angle between the LOS vector and the coordinate axes depends only on the rotation transformation, not the translation. Through the four rotations in Figure 1, the vector from the UAV pointing to the target in the ECEF coordinate system can be obtained as follows (hereinafter referred to as the pointing vector):

$$\mathbf{v}_{E,i} = \mathbf{R}^E_{G,i}\mathbf{R}^G_{U,i}\mathbf{R}^U_{B,i}\mathbf{R}^B_{C,i}\mathbf{v}_{C,i}. \tag{3}$$

Subscripts $i = 1, 2$ indicate different UAVs. $\mathbf{R}^B_{C,i}$, $\mathbf{R}^U_{B,i}$, $\mathbf{R}^G_{U,i}$, and $\mathbf{R}^E_{G,i}$ are rotation matrices. The expressions for these rotation matrices are given in Appendix A. Similar to $\mathbf{v}_{C,i}$, the real rotation matrix can also be represented by parameters affected by noise, see Appendix B for details.

Table 1 details the error distributions for various parameters, which are independent of each other. But in the process of $\mathbf{v}_{C,i}$ rotation transformation to $\mathbf{v}_{E,i}$, there are various phenomena of noise coupling. This leads to the fact that the elements that makeup $\mathbf{v}_{E,i}$ may be related.

From Equation (3) and Appendix B, the real pointing vector in the ECEF coordinate system is expressed as:

$$\begin{aligned}\mathbf{v}_{E,i} &= \mathbf{R}^{E}_{G,i}\mathbf{R}^{G}_{U,i}\mathbf{R}^{U}_{B,i}\mathbf{R}^{B}_{C,i}\mathbf{v}_{C,i} \\ &= \left(\tilde{\mathbf{R}}^{E}_{G,i} - \Delta\tilde{\mathbf{R}}^{E}_{G,i}\right)\left(\tilde{\mathbf{R}}^{G}_{U,i} - \Delta\tilde{\mathbf{R}}^{G}_{U,i}\right)\left(\tilde{\mathbf{R}}^{U}_{B,i} - \Delta\tilde{\mathbf{R}}^{U}_{B,i}\right)\left(\tilde{\mathbf{R}}^{B}_{C,i} - \Delta\tilde{\mathbf{R}}^{B}_{C,i}\right)(\tilde{\mathbf{v}}_{C,i} - \Delta\tilde{\mathbf{v}}_{C,i}) \\ &= \tilde{\mathbf{v}}_{E,i} - \Delta\tilde{\mathbf{v}}_{E,i},\end{aligned} \tag{4}$$

where the observation error is $\Delta\tilde{\mathbf{v}}_{E,i} = \tilde{\mathbf{R}}^{E}_{G,i}\tilde{\mathbf{R}}^{G}_{U,i}\tilde{\mathbf{R}}^{U}_{B,i}\tilde{\mathbf{R}}^{B}_{C,i}\Delta\tilde{\mathbf{v}}_{C,i} + \tilde{\mathbf{R}}^{E}_{G,i}\tilde{\mathbf{R}}^{G}_{U,i}\tilde{\mathbf{R}}^{U}_{B,i}\Delta\tilde{\mathbf{R}}^{B}_{C,i}\tilde{\mathbf{v}}_{C,i} + \tilde{\mathbf{R}}^{E}_{G,i}\tilde{\mathbf{R}}^{G}_{U,i}\Delta\tilde{\mathbf{R}}^{U}_{B,i}\tilde{\mathbf{R}}^{B}_{C,i}\tilde{\mathbf{v}}_{C,i} + \tilde{\mathbf{R}}^{E}_{G,i}\Delta\tilde{\mathbf{R}}^{G}_{U,i}\tilde{\mathbf{R}}^{U}_{B,i}\tilde{\mathbf{R}}^{B}_{C,i}\tilde{\mathbf{v}}_{C,i} + \Delta\tilde{\mathbf{R}}^{E}_{G,i}\tilde{\mathbf{R}}^{G}_{U,i}\tilde{\mathbf{R}}^{U}_{B,i}\tilde{\mathbf{R}}^{B}_{C,i}\tilde{\mathbf{v}}_{C,i}$.

After the calibration of the UAV before take-off, the mean of each parameter noise in Table 1 is zero, so it is easy to know that $E[\Delta\tilde{\mathbf{v}}_{E,i}] = 0$. That is, when only the first-order noise term is considered, the estimation of the pointing vector is unbiased.

According to the measurement error of the pointing vector, it is easy to obtain the covariance matrix of $\Delta\tilde{\mathbf{v}}_{E,i}$ as

$$\begin{aligned}\tilde{\mathbf{V}}_i =& E\left[\Delta\tilde{\mathbf{v}}_{E,i}\Delta\tilde{\mathbf{v}}^{T}_{E,i}\right] \\ =& \tilde{\mathbf{R}}^{E}_{G,i}\tilde{\mathbf{R}}^{G}_{U,i}\tilde{\mathbf{R}}^{U}_{B,i}\tilde{\mathbf{R}}^{B}_{C,i}E\left[\Delta\tilde{v}_{C,i}\Delta\tilde{v}^{T}_{C,i}\right]\left(\tilde{\mathbf{R}}^{E}_{G,i}\tilde{\mathbf{R}}^{G}_{U,i}\tilde{\mathbf{R}}^{U}_{B,i}\tilde{\mathbf{R}}^{B}_{C,i}\right)^{T} \\ &+ \tilde{\mathbf{R}}^{E}_{G,i}\tilde{\mathbf{R}}^{G}_{U,i}\tilde{\mathbf{R}}^{U}_{B,i}\mathrm{d}\tilde{\mathbf{R}}^{B}_{C,\alpha_i}\tilde{\mathbf{v}}_{C,i}E[\Delta\tilde{\alpha}_i\Delta\tilde{\alpha}_i]\left(\tilde{\mathbf{R}}^{E}_{G,i}\tilde{\mathbf{R}}^{G}_{U,i}\tilde{\mathbf{R}}^{U}_{B,i}\mathrm{d}\tilde{\mathbf{R}}^{B}_{C,\alpha_i}\tilde{\mathbf{v}}_{C,i}\right)^{T} \\ &+ \cdots \\ &+ \mathrm{d}\tilde{\mathbf{R}}^{E}_{G,\lambda_i}\tilde{\mathbf{R}}^{G}_{U,i}\tilde{\mathbf{R}}^{U}_{B,i}\tilde{\mathbf{R}}^{B}_{C,\beta_i}\tilde{\mathbf{v}}_{C,i}E\left[\Delta\tilde{M}_i\Delta\tilde{M}_i\right]\left(\mathrm{d}\tilde{\mathbf{R}}^{E}_{G,\lambda_i}\tilde{\mathbf{R}}^{G}_{U,i}\tilde{\mathbf{R}}^{U}_{B,i}\tilde{\mathbf{R}}^{B}_{C,\beta_i}\tilde{\mathbf{v}}_{C,i}\right)^{T},\end{aligned} \tag{5}$$

where $\mathrm{d}\tilde{\mathbf{R}}_{*}$ is the error of the rotation matrix represented by the noisy measurement, see Appendix B.

So far, the pointing vector can be represented by the measurements in the ECEF coordinate system whose distribution satisfies $\tilde{\mathbf{v}}_{E,i} \sim \mathcal{N}\left(\mathbf{v}_{E,i}, \tilde{\mathbf{V}}_i\right)$. Next, we estimate the AOA of the target relative to the UAV in the ECEF coordinate system $\tilde{\mathbf{v}}_{E,i}$.

To be convenient, the pointing vector is expressed as $\tilde{\mathbf{v}}_{E,i} = [\tilde{v}_{i,1}, \tilde{v}_{i,2}, \tilde{v}_{i,3}, 1]^{T}$. The azimuth and elevation of the target observed by the UAV are, respectively,

$$\begin{cases} \tilde{\rho}_i = \arctan\frac{\tilde{v}_{i,2}}{\tilde{v}_{i,1}} \\ \tilde{o}_i = \arctan\frac{\tilde{v}_{i,3}}{\sqrt{\tilde{v}^2_{i,1}+\tilde{v}^2_{i,2}}} \end{cases} \tag{6}$$

Writing AOA in vector form is $\tilde{\mathbf{m}}_i = [\tilde{\rho}_i, \tilde{o}_i]^{T}$. The estimation error of the pointing vector will be passed to AOA through Equation (6). Similar to Equation (4), the estimation error of AOA obtained by only considering the first-order noise term is

$$\Delta\tilde{\mathbf{m}}_i = \tilde{\mathbf{M}}_i\Delta\tilde{\mathbf{v}}_{E,i} \tag{7}$$

where $\Delta\tilde{\mathbf{m}}_i = [\Delta\tilde{\rho}_i, \Delta\tilde{o}_i]^{T}$,

$$\tilde{\mathbf{M}}_i = \frac{1}{\tilde{v}^2_{i,1}+\tilde{v}^2_{i,2}}\begin{bmatrix} -\tilde{v}_{i,2} & \tilde{v}_{i,1} & 0 & 0 \\ \frac{-\tilde{v}_{i,1}\tilde{v}_{i,3}\left(\tilde{v}^2_{i,1}+\tilde{v}^2_{i,2}\right)^{3/2}}{\tilde{v}^2_{i,1}+\tilde{v}^2_{i,2}+\tilde{v}^2_{i,3}} & \frac{-\tilde{v}_{i,2}\tilde{v}_{i,3}\left(\tilde{v}^2_{i,1}+\tilde{v}^2_{i,2}\right)^{3/2}}{\tilde{v}^2_{i,1}+\tilde{v}^2_{i,2}+\tilde{v}^2_{i,3}} & \frac{\left(\tilde{v}^2_{i,1}+\tilde{v}^2_{i,2}\right)^{3/2}}{\tilde{v}^2_{i,1}+\tilde{v}^2_{i,2}+\tilde{v}^2_{i,3}} & 0 \end{bmatrix}.$$

Obviously, the bias of the estimate of AOA is

$$E[\Delta\tilde{\mathbf{m}}_i] = \tilde{\mathbf{M}}_iE[\Delta\tilde{\mathbf{v}}_{E,i}] = 0. \tag{8}$$

The elements in the pointing vector give the AOA from Equation (6), such that the azimuth and elevation are related. Similar to Equation (5), the covariance matrix of AOA estimation error can be expressed as

$$\begin{aligned}\mathbf{Q}_i =& E\left[\Delta\tilde{\mathbf{m}}_i \Delta\tilde{\mathbf{m}}_i^T\right] \\ =& \tilde{\mathbf{M}}_i \tilde{\mathbf{V}}_i \tilde{\mathbf{M}}_i^T.\end{aligned} \tag{9}$$

The estimation of AOA is obtained from the pointing vector through Equations (3) and (6), and many parameters are involved in the whole process. According to the central limit theorem, it can be approximately considered that the estimation of AOA satisfies $\tilde{\mathbf{m}}_i \sim \mathcal{N}(\mathbf{m}_i, \mathbf{Q}_i)$. Azimuth and elevation are related, and $\mathbf{Q_i}$ is a symmetric matrix but not a diagonal matrix.

2.2. The Position of UAV in ECEF Coordinate System

The UAV is equipped with GPS to determine its position in real-time. The GPS outputs the position $\mathbf{t}_i = (M_i, L_i, H_i)^T$ of the UAV in the WGS84 coordinate system, where the parameters represent latitude, longitude, and altitude, respectively. Their noise distributions are shown in Table 1. The components in $\mathbf{t}_i$ are independent of each other, and their covariance matrix is $\mathbf{P}_i = \mathrm{diag}\left(\left[\sigma_{M_i}^2, \sigma_{L_i}^2, \sigma_{H_i}^2\right]\right)$.

In the WGS84 coordinate system, the semi-major axis a = 6,378,137 m, the semi-minor axis b = 6,356,752 m, and the first eccentricity $e = \frac{\sqrt{a^2-b^2}}{a}$. According to the definition of the WGS84 and the ECEF coordinate system, the position $\mathbf{s}_i = (x_i, y_i, z_i)^T$ of the UAV in the ECEF coordinate system is represented by $\mathbf{t}_i$ as [23]

$$\begin{aligned} x_i &= (N_i + H_i)\cos M_i \cos L_i, \\ y_i &= (N_i + H_i)\cos M_i \sin L_i, \\ z_i &= \left(N_i\left(1 - e^2\right) + H_i\right)\sin M_i. \end{aligned} \tag{10}$$

where $N_i = a/w_i$, $w_i = \sqrt{1 - e^2 \sin^2 M_i}$.

Considering the first-order noise of GPS measurements and expressing the UAV position error in the ECEF coordinate system in a fully differential form

$$\begin{aligned}\Delta\mathbf{s}_i =& \frac{\partial \mathbf{s}_i}{\partial M_i}\Delta M_i + \frac{\partial \mathbf{s}_i}{\partial L_i}\Delta L_i + \frac{\partial \mathbf{s}_i}{\partial H_i}\Delta H_i \\ =& \mathbf{K}_i \Delta\mathbf{t}_i\end{aligned} \tag{11}$$

where $\Delta\mathbf{t}_i = (\Delta M_i, \Delta L_i, \Delta H_i)^T$,
$\mathbf{K}_i = \begin{bmatrix} \left[a\left(e^2-1\right)w_i{}^{-3} - H_i\right]\sin M_i \cos L_i & -(N_i + H_i)\cos M_i \sin L_i & \cos M_i \cos L_i \\ \left[a\left(e^2-1\right)w_i{}^{-3} - H_i\right]\sin M_i \sin L_i & (N_i + H_i)\cos M_i \cos L_i & \cos M_i \sin L_i \\ a\cos M_i\left(1-e^2\right)w_i{}^{-3} + H_i \cos M_i & 0 & \sin M_i \end{bmatrix}$ is the Jacobian matrix of $\mathbf{s}_i$ with respect to $\mathbf{t}_i^T$.

The error of the UAV position estimation in the ECEF coordinate system satisfies $E[\Delta\mathbf{s}_i] = 0$, and its covariance matrix is

$$\mathbf{Q}_{s_i} = E\left[\Delta\mathbf{s}_i \Delta\mathbf{s}_i^T\right] = \mathbf{K}_i \mathbf{P}_i {\mathbf{K}_i}^T. \tag{12}$$

So far, the AOA estimation of the target relative to the UAV and the position estimation of the UAV in the ECEF coordinate system has been completed. The next section estimates the target position based on this information.

3. The Proposed Weighted Least Squares Algorithm

The positions of the two UAVs and the AOAs relative to the UAVs for the target are known; the target position can be calculated through simple triangulation. Due to the observation errors in the AOA and UAV positions, the two pointing vectors generally do not intersect at a single point. In [14], the ordinary least squares (OLS) algorithm and adaptive Kalman filtering (KF) algorithm were used to estimate the target position. However, the adaptive KF requires iteration, resulting in higher computational complexity. In this section, we propose an estimation algorithm with a closed-form solution.

3.1. Formulate the Localization Problem

Consider the localization scenario as shown in Figure 2. Two UAVs are loaded with optoelectronic platforms, and $\mathbf{s}_i = [x_i, y_i, z_i]^T$ is known; they use the azimuth angle ρ_i and elevation angle o_i to locate the unknown target $\mathbf{u} = [x_t, y_t, z_t]^T$, where $i = 1, 2$.

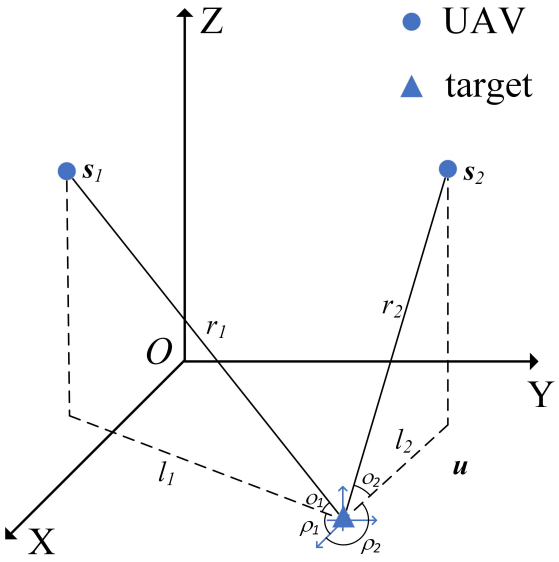

Figure 2. AOA-based localization model for dual UAVs.

The azimuth and elevation are represented by the positions of the UAV and the target as

$$\begin{cases} \rho_i = \arctan \frac{y_t - y_i}{x_t - x_i} \\ o_i = \arctan \frac{z_t - z_i}{l_i} \end{cases} \tag{13}$$

where $l_i = \|\mathbf{s}_i(1:2) - \mathbf{u}(1:2)\| = (x_t - x_i)\cos\rho_i + (y_t - y_i)\sin\rho_i$ is the horizontal distance from the UAV to the target. *arctan* is the arc tangent function.

The AOA is a nonlinear function with respect to the target position, which is difficult to estimate directly. Linearizing Equation (12) to obtain the linear equation about the target position

$$\begin{cases} \sin\rho_i x_t - \cos\rho_i y_t = \sin\rho_i x_i - \cos\rho_i y_i, \\ \cos\rho_i \sin o_i x_t + \sin\rho_i \sin o_i y_t - \cos o_i z_t = \cos\rho_i \sin o_i x_i + \sin\rho_i \sin o_i y_i - \cos o_i z_i. \end{cases} \tag{14}$$

In matrix form, writing Equation (14) as a pseudolinear equation about $\mathbf{u}$

$$\mathbf{A}\mathbf{u} = \mathbf{b} \tag{15}$$

where $\mathbf{A} = \begin{bmatrix} \sin\rho_1 & -\cos\rho_1 & 0 \\ \cos\rho_1 \sin o_1 & \sin\rho_1 \sin o_1 & -\cos o_1 \\ \sin\rho_2 & -\cos\rho_2 & 0 \\ \cos\rho_2 \sin o_2 & \sin\rho_2 \sin o_2 & -\cos o_2 \end{bmatrix}$, $\mathbf{b} = \begin{bmatrix} \mathbf{A}(1:2,:)\mathbf{s}_1 \\ \mathbf{A}(3:4,:)\mathbf{s}_2 \end{bmatrix}$. $\mathbf{A}(1:2,:)$ is a matrix consisting of the first two rows of elements of $\mathbf{A}$.

3.2. The Proposed Weighted Least Squares Estimator

The noise in the observation process cannot be ignored. Now the regression factor $\tilde{\mathbf{A}}$ and the regressor $\tilde{\mathbf{b}}$ are represented by the measurement disturbed by the noise and combined with Equation (15) to obtain

$$\begin{aligned} \left(\tilde{\mathbf{A}} - \Delta\tilde{\mathbf{A}}\right)\mathbf{u} &= \tilde{\mathbf{b}} - \Delta\tilde{\mathbf{b}} \\ \Leftrightarrow \tilde{\mathbf{b}} - \tilde{\mathbf{A}}\mathbf{u} &= \Delta\tilde{\mathbf{b}} - \Delta\tilde{\mathbf{A}}\mathbf{u} \end{aligned} \tag{16}$$

Considering only the first-order noise, it is easy to obtain the error term of the regression equation as

$$\begin{aligned} \mathbf{e} &= \Delta\tilde{\mathbf{b}} - \Delta\tilde{\mathbf{A}}\mathbf{u} \\ &= \tilde{\mathbf{F}}\Delta\tilde{\mathbf{m}} + \tilde{\mathbf{B}}\Delta\tilde{\mathbf{s}} \end{aligned} \tag{17}$$

where $\tilde{\mathbf{F}} = \mathrm{diag}([\tilde{r}_1 \cos\tilde{o}_1, \tilde{r}_1, \tilde{r}_2 \cos\tilde{o}_2, \tilde{r}_2])$, $\tilde{r}_i = \|\tilde{\mathbf{s}}_i - \mathbf{u}\|$, $\Delta\tilde{\mathbf{m}} = \left[\Delta\tilde{\mathbf{m}}_1^T, \Delta\tilde{\mathbf{m}}_2^T\right]^T$, $\Delta\tilde{\mathbf{s}} = \left[\Delta\tilde{\mathbf{s}}_1^T, \Delta\tilde{\mathbf{s}}_2^T\right]^T$, $\tilde{\mathbf{B}} = \mathrm{blkdiag}\left(\tilde{\mathbf{A}}(1:2,:), \tilde{\mathbf{A}}(3:4,:)\right)$.

The positions of each UAV and AOAs are independent of each other. The covariance matrix of $\Delta\mathbf{s}$ is $\mathbf{Q}_s = \mathrm{blkdiag}\left(\mathbf{Q}_{s_1}, \mathbf{Q}_{s_2}\right)$. The covariance matrix of $\Delta\mathbf{m}$ is $\mathbf{Q}_m = \mathrm{blkdiag}(\mathbf{Q}_1, \mathbf{Q}_2)$. The covariance matrix of AOA measurement is related to the parameters in the rotation transformation process, and the covariance matrix of AOA estimated by the UAV is different in different states.

From Equations (16) and (17), it is easy to obtain the weighted least squares estimation (WLSE) of $\mathbf{u}$ as

$$\begin{aligned} \hat{\mathbf{u}} &= \arg\min\left(\tilde{\mathbf{A}}\mathbf{u} - \tilde{\mathbf{b}}\right)\mathbf{W}\left(\tilde{\mathbf{A}}\mathbf{u} - \tilde{\mathbf{b}}\right)^T \\ &= \left(\tilde{\mathbf{A}}^T\mathbf{W}\tilde{\mathbf{A}}\right)^{-1}\tilde{\mathbf{A}}^T\mathbf{W}\tilde{\mathbf{b}} \end{aligned} \tag{18}$$

where $\hat{\mathbf{u}}$ represents the estimation of target position, and $\mathbf{W} = \left(E\left[\mathbf{e}\mathbf{e}^T\right]\right)^{-1} = \left(\mathbf{F}\mathbf{Q}_m\mathbf{F}^T + \mathbf{B}\mathbf{Q}_s\mathbf{B}^T\right)^{-1}$ is the weighting matrix.

The difference between WLS and OLS lies in the weighting matrix, which determines the weight of different error levels. When there is a significant difference in error levels, WLS exhibits significantly improved performance compared to OLS. If the error matrix does not exhibit heteroscedasticity, the performance of WLS is similar to that of OLS.

According to Equation (17), the calculation of the weighting matrix requires the true target position, which is unknown. It can be estimated using an iterative WLSE. Initially, the weighting matrix is roughly calculated using the estimation results from OLS. Then, this weighting matrix is used in Equation (18) to estimate a more accurate target position and then update itself. Typically, this process is repeated two to three times.

3.3. Performance Analysis

We have obtained target position estimates using the proposed WLSE. In the following, the performance of the proposed estimator is evaluated through theoretical analysis from two aspects of the mean and covariance of the estimation error.

Equation (17) is approximately feasible when the following small noise conditions are satisfied: (1) $\Delta\rho_i/\rho_i \simeq 0$; (2) $\Delta o_i/o_i \simeq 0$; (3) $\left\|\mathrm{diag}(\mathbf{s}_i)^{-1}\Delta\mathbf{s}_i\right\| \simeq 0$ for $i = 1, 2$.

From Equation (18), the estimation bias of the target position is

$$\begin{aligned}\Delta\mathbf{u} =&\hat{\mathbf{u}} - \mathbf{u}\\ =&\left(\tilde{\mathbf{A}}^T\mathbf{W}\tilde{\mathbf{A}}\right)^{-1}\tilde{\mathbf{A}}^T\mathbf{W}\tilde{\mathbf{b}} - \left(\tilde{\mathbf{A}}^T\mathbf{W}\tilde{\mathbf{A}}\right)^{-1}\tilde{\mathbf{A}}^T\mathbf{W}\tilde{\mathbf{A}}\mathbf{u}\\ =&\left(\tilde{\mathbf{A}}^T\mathbf{W}\tilde{\mathbf{A}}\right)^{-1}\tilde{\mathbf{A}}^T\mathbf{W}(\mathbf{F}\Delta\mathbf{m} + \mathbf{B}\Delta\mathbf{s})\end{aligned} \tag{19}$$

Section 2 has proved that $E[\Delta\mathbf{s}] = 0$ and $E[\Delta\mathbf{m}] = 0$. Obviously, the mean of the estimation bias satisfies $E[\Delta\mathbf{u}] = 0$, which means that the WLSE of the target position is unbiased.

From (19), the covariance matrix of the estimation error is

$$\begin{aligned}\mathrm{cov}(\Delta\mathbf{u}) =&E\left[\Delta\mathbf{u}\Delta\mathbf{u}^T\right]\\ =&\left(\tilde{\mathbf{A}}^T\mathbf{W}\tilde{\mathbf{A}}\right)^{-1}\tilde{\mathbf{A}}^T\mathbf{W}\mathbf{F}E\left[\Delta\mathbf{m}\Delta\mathbf{m}^T\right]\left(\left(\tilde{\mathbf{A}}^T\mathbf{W}\tilde{\mathbf{A}}\right)^{-1}\tilde{\mathbf{A}}^T\mathbf{W}\mathbf{F}\right)^T\\ =&\left(\tilde{\mathbf{A}}^T\mathbf{W}\tilde{\mathbf{A}}\right)^{-1} \simeq \left(\mathbf{A}^T\mathbf{W}\mathbf{A}\right)^{-1}\\ =&\left(\mathbf{A}^T\left(\mathbf{F}\mathbf{Q}_\mathbf{m}\mathbf{F}^T + \mathbf{B}\mathbf{Q}_\mathbf{s}\mathbf{B}^T\right)^{-1}\mathbf{A}\right)^{-1}\end{aligned} \tag{20}$$

It is described in the Introduction that CRLB is the lower bound of the variance of the unbiased estimate, which is often used to evaluate the performance of the algorithm. The performance of the proposed estimator can be verified by comparing the CRLB and $\mathrm{cov}(\Delta\mathbf{u})$.

During the localization process, the measurement errors of the UAV position and AOA jointly affect the accuracy of target position estimation. The AOA and UAV positions are unified into a vector form as $\mathbf{m_t} = \left[\mathbf{m}^T, \mathbf{s}^T\right]^T$, and the target position and the UAV position are written in vector form $\mathbf{f} = \left[\mathbf{u}^T, \mathbf{s}^T\right]^T$.

According to $\mathbf{m_t}$, the FIM of $\mathbf{f}$ is [24]

$$\mathbf{\Phi} = \begin{bmatrix} \mathbf{J}_\mathbf{u}^T\mathbf{Q}_\mathbf{m}^{-1}\mathbf{J}_\mathbf{u} & \mathbf{J}_\mathbf{u}^T\mathbf{Q}_\mathbf{m}^{-1}\mathbf{J}_\mathbf{s} \\ \mathbf{J}_\mathbf{s}^T\mathbf{Q}_\mathbf{m}^{-1}\mathbf{J}_\mathbf{u} & \mathbf{J}_\mathbf{s}^T\mathbf{Q}_\mathbf{m}^{-1}\mathbf{J}_\mathbf{s} + \mathbf{Q}_\mathbf{s}^{-1} \end{bmatrix} \tag{21}$$

where $\mathbf{J}_u$ and $\mathbf{J_s}$ are the Jacobians of $\mathbf{m}$ relative to $\mathbf{u}^T$ and $\mathbf{s}^T$, respectively. $\mathbf{J_u} = \frac{\partial\mathbf{m}}{\partial\mathbf{u}^T} = \begin{bmatrix} \frac{\sin\rho_1}{r_1\cos o_1} & -\frac{\cos\rho_1}{r_1\cos o_1} & 0 \\ \frac{\cos\rho_1\sin o_1}{r_1} & \frac{\sin\rho_1\sin o_1}{r_1} & -\frac{\cos o_1}{r_1} \\ \frac{\sin\rho_2}{r_2\cos o_2} & -\frac{\cos\rho_2}{r_2\cos o_2} & 0 \\ \frac{\cos\rho_2\sin o_2}{r_2} & \frac{\sin\rho_2\sin o_2}{r_2} & -\frac{\cos o_2}{r_2} \end{bmatrix}$, $\mathbf{J_s} = \frac{\partial\mathbf{m}}{\partial\mathbf{s}^T} = \mathrm{blkdiag}(-\mathbf{J_u}(1:2,:), -\mathbf{J_u}(3:4,:))$.

When the measurement noise follows a Gaussian distribution,

$$\mathrm{CRLB}(\mathbf{f}) = \mathbf{\Phi}^{-1}, \tag{22}$$

where the 3×3 part of the upper left corner of $\mathrm{CRLB}(\mathbf{f})$ is the CRLB of the target position estimate. The 6×6 block matrix in the lower right corner of the FIM is an invertible matrix, and the CRLB of the target position estimate obtained by using the matrix inversion formula [25] is

$$\mathrm{CRLB}(\mathbf{u}) = \left(\mathbf{J}_\mathbf{u}^T\mathbf{Q}_\mathbf{m}^{-1}\mathbf{J}_\mathbf{u} - \mathbf{J}_\mathbf{u}^T\mathbf{Q}_\mathbf{m}^{-1}\mathbf{J}_\mathbf{s}\left(\mathbf{J}_\mathbf{s}^T\mathbf{Q}_\mathbf{m}^{-1}\mathbf{J}_\mathbf{s} + \mathbf{Q}_\mathbf{s}^{-1}\right)^{-1}\mathbf{J}_\mathbf{s}^T\mathbf{Q}_\mathbf{m}^{-1}\mathbf{J}_\mathbf{u}\right)^{-1}. \tag{23}$$

According to Equation (20), the covariance matrix of the target position estimation error can be expressed as

$$\begin{aligned}\operatorname{cov}(\Delta\mathbf{u}) \simeq & \left(\mathbf{A}^T\left(\mathbf{F}\mathbf{Q}_\mathbf{m}\mathbf{F}^T+\mathbf{B}\mathbf{Q}_\mathbf{s}\mathbf{B}^T\right)^{-1}\mathbf{A}\right)^{-1} \\ =&\mathbf{A}^T\mathbf{F}^{-T}\mathbf{Q}_\mathbf{m}^{-1}\mathbf{F}^{-1}\mathbf{A} \\ &-\mathbf{A}^T\mathbf{F}^{-T}\mathbf{Q}_\mathbf{m}^{-1}\mathbf{F}^{-1}\mathbf{B}\left(\mathbf{Q}_\mathbf{s}^{-1}+\mathbf{B}^T\mathbf{F}^{-T}\mathbf{Q}_\mathbf{m}^{-1}\mathbf{F}^{-1}\mathbf{B}\right)^{-1}\mathbf{B}^T\mathbf{F}^{-T}\mathbf{Q}_\mathbf{m}^{-1}\mathbf{F}^{-1}\mathbf{A}.\end{aligned} \tag{24}$$

From the definition of matrix $\mathbf{F}$, $\mathbf{A}$, $\mathbf{B}$, $\mathbf{J_u}$, and $\mathbf{J_s}$ in Equations (17) and (21), there is an equality relationship $\mathbf{F}^{-1}\mathbf{A}=\mathbf{J_u}$ and $\mathbf{F}^{-1}\mathbf{B}=-\mathbf{J_s}$. Substituting into Equations (23) and (24), it is obvious that the covariance matrix and CRLB of the target position estimation satisfy

$$\operatorname{cov}(\mathbf{u}) \simeq \mathrm{CRLB} \tag{25}$$

In summary, only the first-order noise term is considered under the condition of small noise, the target position estimator proposed in this paper is approximately unbiased, and the covariance matrix of the estimation error can reach CRLB.

4. Optimal Placement of Coplanar UAVs Relative to Target

In addition to the localization algorithm, the placement of the UAVs relative to the target has a great influence on the estimation accuracy of the target position. In the process of passive localization, in order to avoid exposure, the UAVs need to keep a certain distance $r_i \geq L$ from the target, where L represents a minimum safe distance. For the convenience of analysis, it is assumed that the flying heights of the two UAVs are equal and the distance to the target is the same, that is, $z_1 = z_2$ and $r_1 = r_2$. In this section, based on the D-optimality criterion, the optimal placement of two coplanar UAVs relative to the target is studied.

The determinant of CRLB represents the volume of the target position estimation error ellipsoid, and the minimization of the error ellipsoid volume is an intuitive optimization goal. When the noise obeys Gaussian distribution, CRLB and FIM are mutually inverse. The determinant of these two matrices satisfies

$$\det(\mathrm{CRLB}) = \det(\mathrm{FIM})^{-1}. \tag{26}$$

With minimizing det(CRLB) and maximizing det(FIM), as the objective function to optimize the layout between the UAVs and the target to achieve high-precision localization.

When the UAVs are located on the same horizontal plane, the height difference between the target and the UAVs is $h = z_i - z_t$. The horizontal distance and spatial distance between the target and the UAV satisfy $l = \frac{h}{\tan o}$ and $r = \frac{h}{\sin o}$, respectively. det(FIM) of the target-UAVs geometry is translation-invariant in 3D space and rotation-invariant around the z-axis [22]. When only two UAVs are involved in locating the target, the horizontal placement of the two UAVs relative to the target can be represented by the separation angle λ of the two azimuths. For the convenience of analysis, take the target position as the origin of the coordinates. Let the azimuths of the target relative to the UAVs $\mathbf{s}_1$ and $\mathbf{s}_2$ be $\rho_1 = 0$ and $\rho_2 = \lambda$, respectively, as shown in Figure 3. In Section 2, the variance of the AOA has been obtained through the error transfer model. The variances of the azimuth and elevation are related to various parameters when the UAV locates the target. Set the ratio of elevation to the azimuth error standard deviation as $k = \sigma_o/\sigma_\rho$ ($k > 0$, hereinafter referred to as the noise ratio).

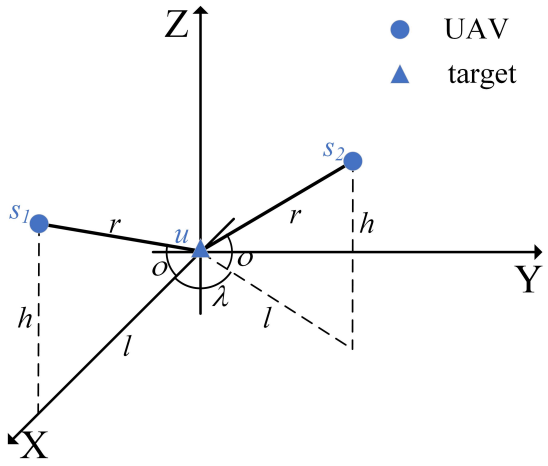

Figure 3. The geometry between the two UAVs and the target.

The two UAVs independently observe the target. The inverse of the covariance matrix of $\Delta\mathbf{m}$ is

$$\mathbf{Q}_m^{-1} = \text{blkdiag}\left(\mathbf{Q}_1^{-1}, \mathbf{Q}_2^{-1}\right) \tag{27}$$

where $\mathbf{Q}_i^{-1} = \frac{1}{\sigma_{\rho i}^2\sigma_{oi}^2 - \sigma_{\rho ioi}^2}\begin{bmatrix}\sigma_{oi}^2 & \sigma_{\rho ioi}\\ \sigma_{\rho ioi} & \sigma_{\rho i}^2\end{bmatrix}$. $\sigma_{\rho i}^2$ and σ_{oi}^2 are the variances of the azimuth and elevation, respectively. $\sigma_{\rho ioi}$ is the covariance of the azimuth and elevation.

In 3D space, the FIM based on AOA localization is [22]

$$\mathbf{\Phi} = \mathbf{\Phi}_1 + \mathbf{\Phi}_2 + \mathbf{\Phi}_3 + \mathbf{\Phi}_4, \tag{28}$$

where $\mathbf{\Phi}_1 = q_1\begin{bmatrix}\sin^2\lambda & -\frac{1}{2}\sin 2\lambda & 0\\ -\frac{1}{2}\sin 2\lambda & 1+\cos^2\lambda & 0\\ 0 & 0 & 0\end{bmatrix}$, $q_1 = \frac{\sigma_o^2\tan^2 o}{h^2\left(\sigma_o^2\sigma_v^2 - \sigma_{ov}^2\right)}$,

$\mathbf{\Phi}_2 = q_2\begin{bmatrix}1+\cos^2\lambda & \frac{1}{2}\sin 2\lambda & -\cot o(1+\cos\lambda)\\ \frac{1}{2}\sin 2\lambda & \sin^2\lambda & -\cot o\sin\lambda\\ -\cot o(1+\cos\lambda) & -\cot o\sin\lambda & 2\cot^2 o\end{bmatrix}$, $q_2 = \frac{\sigma_\rho^2\sin^4 o}{h^2\left(\sigma_o^2\sigma_v^2 - \sigma_{ov}^2\right)}$,

$\mathbf{\Phi}_3 = q_3\begin{bmatrix}\frac{1}{2}\sin 2\lambda & \sin^2\lambda & -\sin\lambda\cot o\\ -1-\cos^2\lambda & -\frac{1}{2}\sin 2\lambda & (1+\cos\lambda)\cot o\\ 0 & 0 & 0\end{bmatrix}$, $q_3 = \frac{\sigma_{ov}\sin^2 o\tan o}{h^2\left(\sigma_o^2\sigma_v^2 - \sigma_{ov}^2\right)}$, $\mathbf{\Phi}_4 = \mathbf{\Phi}_3^T$.

At this time, the geometric optimization problem between the UAVs and the target is expressed in the mathematical form as

$$\begin{aligned}&\max_{\lambda,o}\det(\mathbf{\Phi})\\ &\text{s.t.} o \in [0^\circ, 90^\circ), \lambda \in [-180^\circ, 180^\circ).\end{aligned} \tag{29}$$

There are only two variables in Formula (29); the optimal solution to maximize it can be found by analyzing the convexity of $\det(\mathbf{\Phi})$. When $k > 0$, $\frac{\partial\det(\mathbf{\Phi})}{\partial\cos o} < 0$ is always established. That is to say, in order to maximize the determinant, $\cos o$ should be as small as possible. In the actual localization scenario, the minimum safe distance and maximum flying height of the UAVs will limit the elevation $o \le o_m = \arcsin\frac{h}{L}$. Therefore, the elevation of the optimal placement between the UAVs and the target should satisfy $o = o_m$.

When $0 < k \le \sqrt{2\cos^2 o_m - 2\cos^4 o_m}$, $\frac{\partial\det(\mathbf{\Phi})}{\partial\cos\lambda} < 0$ is always established. To maximize the determinant, $\cos\lambda$ should be as small as possible, and the separation angle $\lambda = 180^\circ$ of the azimuth corresponding to the optimal layout.

When $k > \sqrt{2\cos^2 o_m - 2\cos^4 o_m}$, $\frac{\partial^2 \det(\mathbf{\Phi})}{\partial \cos^2 \lambda} < 0$ is always established. By letting $\frac{\partial \det(\mathbf{\Phi})}{\partial \cos \lambda} = 0$, the separation angle when the determinant is the largest is

$$\lambda = \arccos\left(\frac{\cos^2 o_m\left(\cos^2 o_m - 1\right)}{k^2 - \cos^2 o_m + \cos^4 o_m}\right). \tag{30}$$

So far, the UAV-target optimal placement corresponding to different noise ratios has been found. According to Equation (28), the height difference h between the target and the UAV only affects the value of $\det(\mathbf{\Phi})$ and has nothing to do with the optimal geometry. That is, each noise ratio corresponds to a unique optimal placement.

The research presented in Sections 2–4 are reviewed, the AOA and UAV positions along with their distributions are estimated, the WLS algorithm is proposed, and ultimately the UAV-target deployment is optimized. We have successfully achieved a high-precision cooperative target localization scheme using a dual UAVs system equipped with an opto-electronic platform. The pseudocode below and the flowchart on the next page Figure 4 detail the implementation process of high-precision localization.

Algorithm 1: The scheme of two UAVs using the photoelectric platform to achieve high-precision localization target

Data: Missing amount(x, y), Gimbal angle(α, β),vibration angle$(\phi, \chi, \varepsilon)$, attitude angle$(\kappa, \gamma, \eta)$, GPS$(L, M, H)$, and error distribution of the parameters maximum height h and minimum safety distance L;

Result: High-precision estimation of target position

initialization;
Estimate the AOA of the target relative to the UAV and its noise distribution by formulas Equations (4)–(6) and (8);
Estimate the position of the UAV in the ECEF coordinate system and its noise distribution by formulas Equations (9) and (10);
The maximum pitch angle o_m is determined by the maximum flying height of the UAV and the minimum safe distance between the UAV and the target;
Let $\mathbf{W} = \mathbf{I}_4$; obtain a rough estimate $\tilde{\mathbf{u}}$ of the target position by formula Equation (18);
repeat
    Use $\tilde{\mathbf{u}}$ to update the weighting matrix $\mathbf{W}$, and obtain a more accurate target position estimate $\hat{\mathbf{u}}$ from Equation (18);
until 2–3 times;
Use the noise distribution in step 2 to calculate the noise ratio $k = \sigma_o / \sigma_\rho$ of the AOA;
if $0 < k \leq \sqrt{2\cos^2 o_m - 2\cos^4 o_m}$ **then**
    The separation angle and elevation angle corresponding to the optimal placement are $\lambda = 180^\circ$ and $o = o_m$, respectively;
else
    The optimal separation angle is obtained from Equation (30), and the elevation is o_m;
end
Move the UAVs to the optimal placement relative to the target;
Repeat the above process 2–3 times.

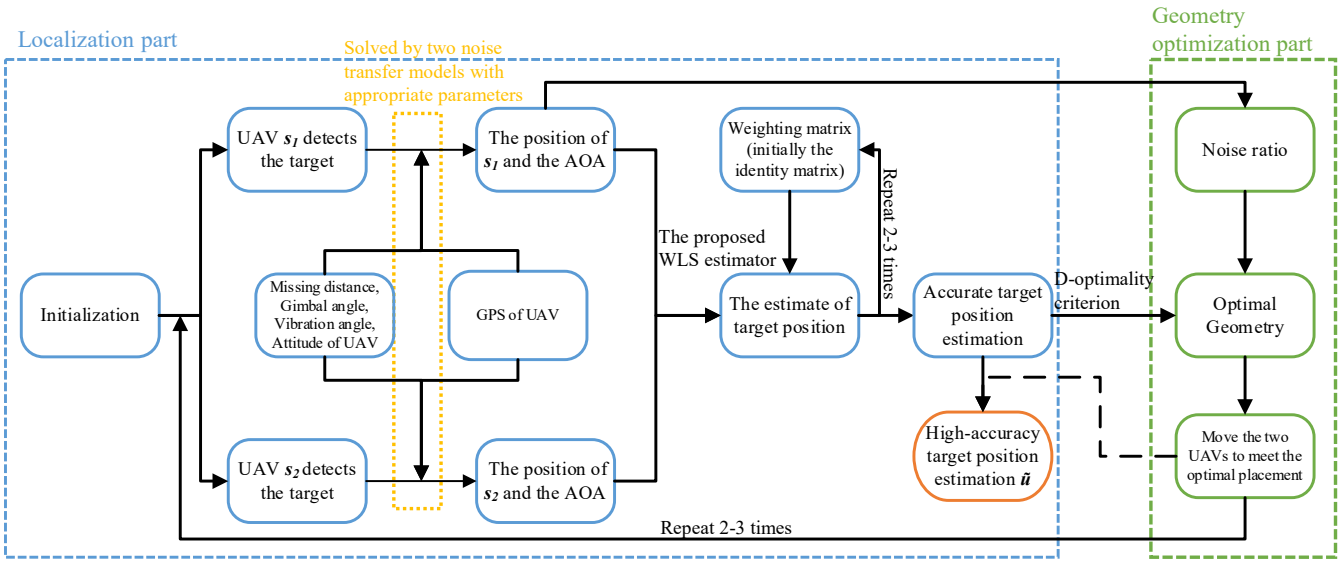

Figure 4. The flowchart corresponding to the pseudocode of Algorithm 1.

5. Simulation and Discussion

This section verifies the accuracy and effectiveness of the theoretical conclusions through a series of simulation experiments and analyzes and discusses the simulation results.

5.1. Estimate the Variances of AOA and UAV Positions

First, the AOA of the target and its error distribution are calculated by the Monte Carlo (MC) method based on the state parameters of the UAV.

Example 1. *The measurements of each subsystem of the UAV are shown in Table 2. The AOA is obtained by Equations (3) and (6) using each noise-disturbed measurement. This process is repeated 5000 times, expressing the values of these AOAs in the form of a histogram and calculating their variances. One of the groups of measurements is selected and substituted into Equation (5) to estimate the variance of AOA. These two variances are compared to demonstrate the validity of the theoretical approach.*

Table 2. Variables used to estimate AOA.

Parameter	Value	Parameter	Value
Missing distance of $x(pixel)$	0	Missing distance of $y(pixel)$	0
Azimuth of gimbal angle(°)	−62.1712	Elevation of gimbal angle(°)	−60.1477
Heading of vibration angle(°)	0	Heading of UAV(°)	0
Pitch of vibration angle(°)	0	Pitch of UAV(°)	0
Yaw of vibration angle(°)	0	Yaw of UAV(°)	0
Longitude of UAV(°)	125.67412	Latitude of UAV(°)	42.13541

In Figures 5 and 6, the probability density distributions of the azimuth and elevation calculated by the two methods are compared. In Figure 5, the variance of the azimuth obtained by the MC method and theoretical calculation is 7.5066×10^{-7} rad^2 and 7.4195×10^{-7} rad^2, respectively. Similarly, the variances of elevation obtained by the two methods in Figure 6 are 1.1424×10^{-6} rad^2 and 1.1320×10^{-6} rad^2 respectively. Simple

calculation shows that the variance estimates of the two methods differ by no more than 3%. This effectively illustrates the accuracy of the theoretical estimate of the AOA variance.

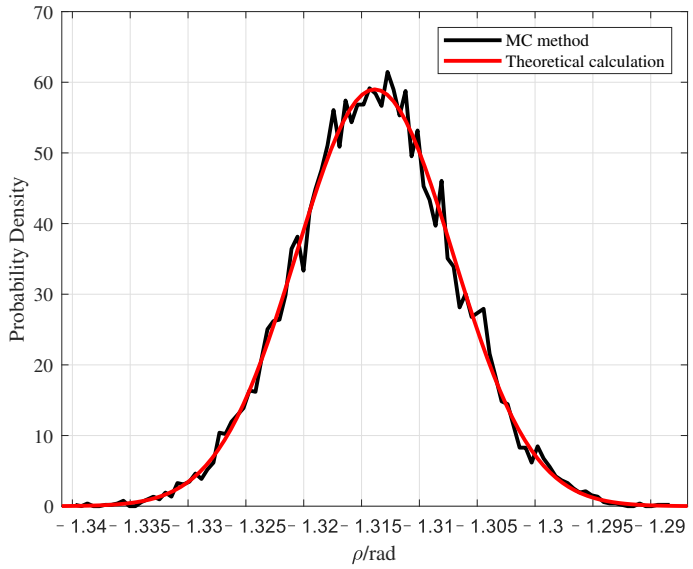

Figure 5. Probability density estimates of azimuths are obtained in two ways.

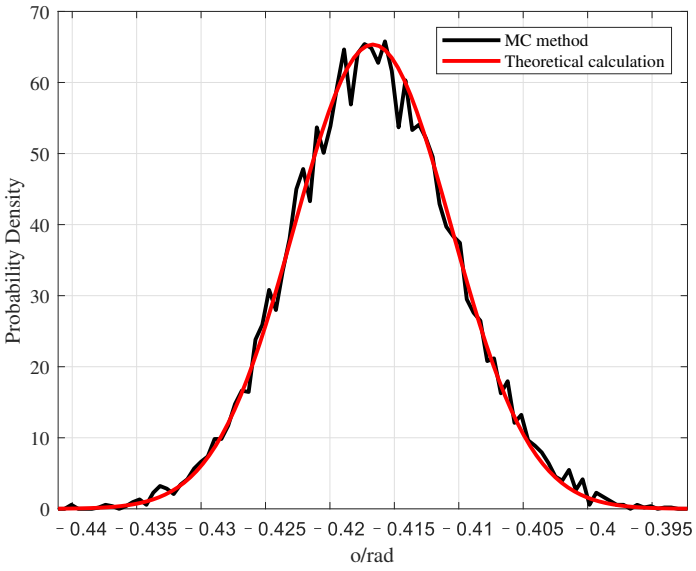

Figure 6. Probability density estimates of elevations are obtained in two ways.

Example 2. *In a similar manner to Example 1, the position of the UAV in the ECEF coordinate system is calculated from measurements in the WGS84 coordinate system. The measurements output by the GPS have a latitude of* 42.1354°*, a longitude of* 125.6741°*, and an altitude of* 6000 m*. Their error distributions are shown in Table 1. Comparing the variance estimation of Equation (11) and the MC method shows the accuracy of the UAV position estimation in the ECEF coordinate system.*

Table 3 describes the variance estimation results corresponding to the two methods. The variance estimates for the three position components were off by less than 3% on average. In this way, the position estimation of UAV in the ECEF coordinate system can also be considered effective.

Table 3. Variances corresponding to MC method and theoretical analysis in the ECEF coordinate system.

The Position Component of the UAV	Variance of the MC Estimate $(\mathbf{m^2})$	Variance of Theoretical Estimate $(\mathbf{m^2})$
x	279.3674	275.2468
y	256.2604	256.0767
z	232.9268	234.8598

5.2. Performance of Localization Algorithms

The accuracy and feasibility of the error estimation of the AOA and UAV positions have been verified in the previous subsection. This section compares with different algorithms and verifies the performance of the proposed WLSE. The performance is evaluated by bias and MSE, which are calculated by

$$\text{bias}(\hat{\mathbf{u}}) = \sum_{i=1}^{n} \frac{(\hat{\mathbf{u}}_i - \mathbf{u})}{n}, \tag{31}$$

$$\mathbf{MSE}(\hat{\mathbf{u}}) = \sum_{i=1}^{n} \frac{\|\hat{\mathbf{u}}_i - \mathbf{u}\|^2}{n}. \tag{32}$$

Example 3. *Using two UAVs with the same configuration to locate the target, the error distribution of the parameters is shown in Table 1. The position of the UAV* $\mathbf{s_1}$ *is the same as in Example 2, and the GPS of* $\mathbf{s_2}$ *is (41.1354°, 125.0741°, 6000 m). The position of the target in the ECEF coordinate system is (−2,746,994 m, −2,503,279 m, 5,162,855 m). The state parameters of the UAV* $\mathbf{s_1}$ *are shown in Table 2 and generate the parameters of* $\mathbf{s_2}$ *according to the target position. Compute the CRLB of the target position estimation based on the variances of the AOA and UAV positions in Examples 1 and 2 as the performance evaluation criterion. And use the OLS estimation as the iteration initial value of MLE.*

The localization performance of different algorithms is shown in Table 4. Comparing the data in Table 4, it is easy to find that the MSE of the proposed algorithm in this paper is similar to MLE and close to CRLB, while the MSE of the OLS estimation is the largest. The bias of the proposed algorithm is larger than that of OLS and MLE but negligible relative to MSE. The running time of MLE is much higher than the proposed algorithm and OLS since MLE is an iterative algorithm with high computational complexity, while both WLS and OLS have closed-form solutions. The above analysis shows that the proposed WLSE has higher accuracy and lower computational complexity.

Table 4. Localization performance of different algorithms.

Algorithm	Running Time (ms)	Bias (m)	MSE $(\mathbf{m^2})$
OLS	0.0128	2.1358	10,065
Proposed algorithm	0.0180	2.6249	6573
MLE	7.1674	1.8918	6588
CRLB	\	\	6583

To further verify the performance of the proposed algorithm in this paper, the AOA and UAV positions under different noise levels are selected to locate the target. There are many parameters that affect AOA, and it is not convenient to obtain the expected AOA noise by adjusting the error of each parameter. Therefore, we choose to directly set different AOA errors and UAV position errors for simulation experiments.

Example 4. *Set the positions of the two UAVs as (2000 m, 1000 m, 2000 m) and (−1000 m, 1000 m, 1000 m). Consider the following two error conditions:* $\sigma_\rho = \sigma_o = 1^\circ$ *and* $\sigma_\rho = 3\sigma_o = 3^\circ$.

The standard deviation of each component error of the UAV position is σ_s. Estimate the position of the target using measurements disturbed by noise with different standard deviations, and repeat the localization process 1000 times. To test for a wider range of errors, the standard deviation of the errors is expressed in logarithmic form.

As shown in Figure 7, when σ_s is small, both the MSEs of the proposed algorithm and MLE can reach CRLB. At this time, the error mainly comes from AOA measurement. The MSE of the OLS estimation in Figure 6a,b are 0.5 dB and 1 dB higher than CRLB, respectively. As σ_s increases, the MSE of various algorithms increases, and the localization performance gradually improves. The weighting matrix in Equation (18) mainly depends on the position error of UAV, and the weight of the AOA error cannot be accurately judged. Comparing (a) and (b), it is easy to find that the larger the noise ratio of AOA, the greater the performance improvement of the algorithm proposed in this paper relative to OLS.

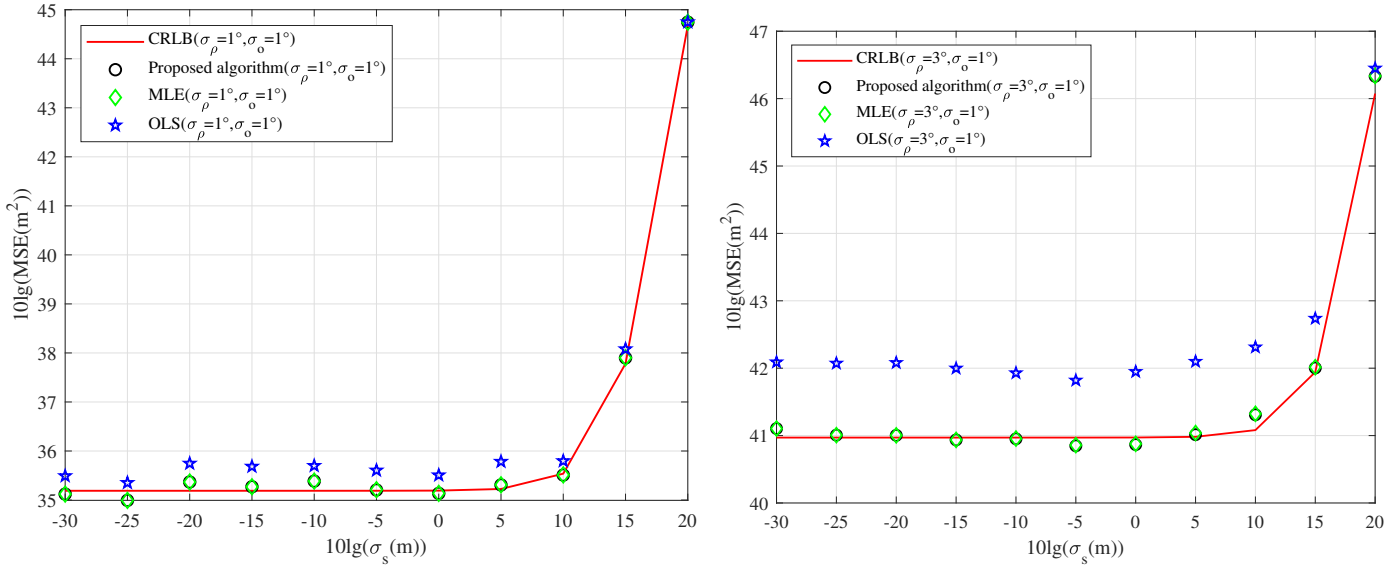

(a) $\sigma_\rho = \sigma_o = 1°$ **(b)** $\sigma_\rho = 3\sigma_o = 3°$

Figure 7. The localization performance of different algorithms varies with σ_s.

Example 5. *The positions of the UAVs and the target are the same as in Example 4. Set the standard deviation of the position error of UAV component to 10 m. The standard deviations of azimuth and elevation consider two cases, respectively: $\sigma_\rho = \sigma_o = \rho°$ and $\sigma_\rho = 3\sigma_o = 3\rho°$. Refer to Example 4 for the localization process.*

In Figure 8, when ρ is small, the MSE of the estimated results of various algorithms can be close to CRLB. As ρ increases, their localization performance gradually deviates from CRLB, and MLE starts to show a threshold effect [26]. In (b), the performance of the proposed algorithm is greater than that of OLS. Because the noise of AOA is larger, the advantage of the weighting matrix is more obvious. When AOA receives too much interference and cannot successfully locate the target, the CRLB at this time has no reference significance.

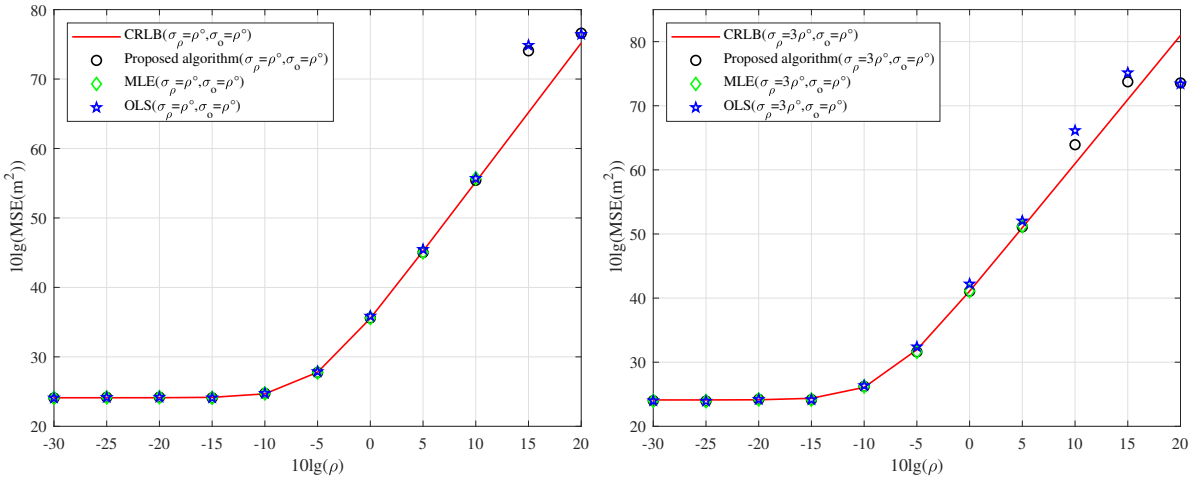

(**a**) $\sigma_\rho = \sigma_o = \rho^\circ$ (**b**) $\sigma_\rho = 3\sigma_o = 3\rho^\circ$

Figure 8. When $\sigma_s = 10$ m, the localization performance of different algorithms changes with ρ.

5.3. Optimize Placement

In Section 4, based on the D-optimality criterion, the optimal layout of relatively stationary target is analyzed when UAVs are located in the same horizontal plane. Below, we design several simulation experiments to verify the accuracy of the theoretical conclusions.

Example 6. *Consider that the noise ratio satisfies* $k = 1$ *and* $k = \sqrt{2}/2$ *, respectively, and set the maximum elevation angle of the target relative to the UAV to be* $o_m = 45^\circ$*. Fix the target and simultaneously move the two UAVs on a spherical surface with the target as the center to change the azimuth and elevation of the target. The optimal placement is verified by comparing the estimation accuracy of the target position corresponding to all optional elevations and separation angles by the exhaustive method at* 1° *intervals.*

When the elevation is constrained, the elevation of the target relative to the UAV in the optimal layout is $o = o_m = 45^\circ$. At the same time, if the noise ratio $k = 1$, according to Equation (30), the separation angle corresponding to the optimal placement is 109.47°. And when the noise ratio $k = \sqrt{2}/2$, the separation angle corresponding to the optimal geometry is 180°. The results in Figure 9 are the same as the theoretical analysis.

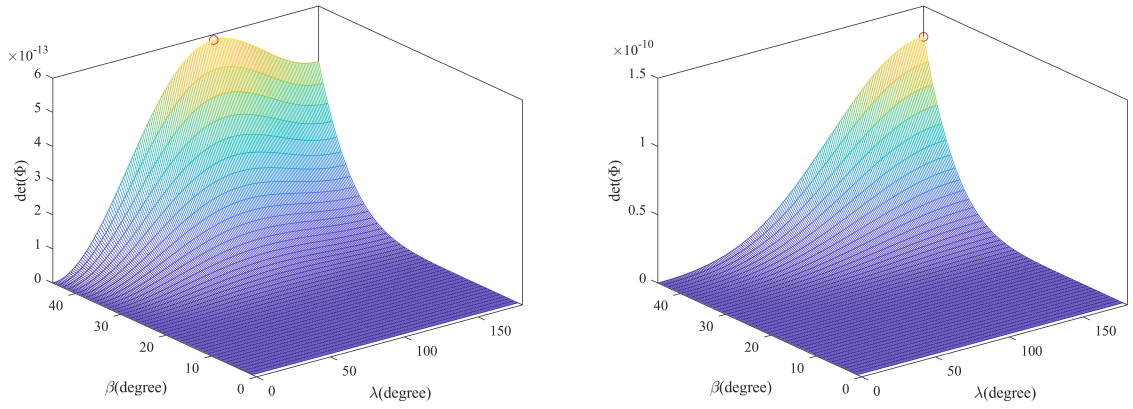

(**a**) $k = 1$ (**b**) $k = \sqrt{2}/2$

Figure 9. det(Φ) corresponding to elevation and separation angle under different noise ratios. The red 'o' indicates the separation angle and elevation that maximize det(Φ).

Example 7. *To further verify the conclusion about the optimal placement, we enumerated the UAV positions corresponding to different elevation and separation angle pairs* $(45°, 45°)$, $(45°, 90°)$, $(45°, 109°)$, $(45°, 135°)$, *and* $(45°, 180°)$. *Set the distance between the UAV and the target as* $r = 1000$ *m, and the measurement noise of AOA is consistent with Example 6. Use the proposed algorithm in this paper and the MLE to locate the target.*

Compare the localization accuracy corresponding to different placements (elevation and separation angle of azimuth) under different noise ratio conditions in Table 5. It is easy to find that the geometric layout corresponding to the smallest estimation error is the same as the theoretical result, which further verifies the accuracy of the conclusions obtained from the theoretical analysis.

Table 5. When the noise ratio $k = 1$ and $k = \sqrt{2}/2$, the localization accuracy of different algorithms is under different configurations.

Noise Ratio	(Elevation, Separation Angle)	CRLB $(\mathbf{m^2})$	Proposed Algorithm $(\mathbf{m^2})$	MLE $(\mathbf{m^2})$
$k = 1$	$(45°, 45°)$	1322	1408	1335
	$(45°, 90°)$	650	665	654
	$(45°, 109°)$	605	612	607
	$(45°, 135°)$	612	645	618
	$(45°, 180°)$	662	674	665
$k = \sqrt{2}/2$	$(45°, 45°)$	2366	2445	2370
	$(45°, 90°)$	960	974	963
	$(45°, 109°)$	836	842	838
	$(45°, 135°)$	770	791	774
	$(45°, 180°)$	755	758	756

In the localization scenario of this paper, since the A-optimality criterion and the D-optimality criterion are not completely equivalent [27], under some UAVs-target placements, the geometric layout obtained according to the D-optimality criterion may not be optimal. However, the performance gap of Tr(CRLB) corresponding to the optimal layout obtained according to these two optimization criteria is negligible, and it is approximately considered that they all satisfy the optimal distribution [28].

6. Conclusions and Future Work

This paper proposes a scheme for locating unknown targets with high precision using dual UAVs loaded with optoelectronic platforms. First, we established an error transfer model for estimating AOA based on the principle of photoelectric platforms detecting targets, and the deviation of the variance of AOA does not exceed 3%. According to the conversion relationship between the WGS84 coordinate system and the ECEF coordinate system, the error transfer model of UAV position in different coordinate systems is established. The noise distribution of the UAV position in the ECEF coordinate system is estimated from the GPS measurements with the deviation of the variance not exceeding 3%. Then, according to the noise distributions of UAV position and AOA, we proposed a WLS algorithm with a closed-form solution. Compared with OLS and MLE, it has the advantages of estimation accuracy and computational complexity. When the variance of AOA differs greatly, WLS can improve the positioning accuracy more. Finally, based on the D-optimality criterion, the placement optimization problem of two coplanar UAVs relative to the target is studied. Through theoretical analysis, the elevation of the UAV relative to the target should be as large as possible, but the separation angle of the azimuth depends on the variance ratio of the azimuth and the elevation. The effectiveness of the localization scheme is verified by a series of simulation experiments.

However, the research goal of this paper is to locate a single stationary target; it does not need to consider the speed of the target and the path planning of the UAVs. Moreover, the research conclusions about optimal placement have limited the usage scenarios and cannot be extended to arbitrary 3D localization scenarios. In the future, we will conduct further research on these matters.

Author Contributions: Conceptualization, X.K. and Y.S.; Methodology, X.K., Y.S. and G.B.; Software, X.K.; Validation, X.K.; Formal analysis, X.K.; Resources, H.S. and D.W.; Data curation, G.B. and T.Z.; Writing—original draft, X.K.; Writing—review & editing, T.Z. and D.W.; Visualization, T.Z.; Project administration, D.W.; Funding acquisition, H.S. and D.W. All authors have read and agreed to the published version of the manuscript.

Funding: This research was funded by the National Natural Science Foundation of China under Grant 62205332.

Institutional Review Board Statement: Not applicable.

Informed Consent Statement: Not applicable.

Data Availability Statement: No new data were created.

Conflicts of Interest: The authors declare no conflict of interest.

Appendix A. Rotation Matrix between Different Coordinate Systems

The rotation matrix of the camera coordinate system to the base coordinate system:

$$\mathbf{R}_{C,i}^{B} = \mathbf{R}_r \mathbf{R}_{\alpha,i} \mathbf{R}_{\beta,i}, \tag{A1}$$

$$\text{where} \quad \mathbf{R}_{\alpha,i} = \begin{bmatrix} \cos\alpha_i & -\sin\alpha_i & 0 & 0 \\ \sin\alpha_i & \cos\alpha_i & 0 & 0 \\ 0 & 0 & 1 & 0 \\ 0 & 0 & 0 & 1 \end{bmatrix}, \quad \mathbf{R}_{\beta,i} = \begin{bmatrix} 1 & 0 & 0 & 0 \\ 0 & \cos\beta_i & \sin\beta_i & 0 \\ 0 & -\sin\beta_i & \cos\beta_i & 0 \\ 0 & 0 & 0 & 1 \end{bmatrix},$$

$$\mathbf{R}_r = \begin{bmatrix} 0 & 0 & 1 & 0 \\ 1 & 0 & 0 & 0 \\ 0 & 1 & 0 & 0 \\ 0 & 0 & 0 & 1 \end{bmatrix}.$$

The rotation matrix from the base coordinate system to the UAV coordinate system:

$$\mathbf{R}_{B,i}^{U} = \mathbf{R}_{\phi,i} \mathbf{R}_{\chi,i} \mathbf{R}_{\varepsilon,i}, \tag{A2}$$

$$\text{where } \mathbf{R}_{\phi,i} = \begin{bmatrix} \cos\phi_i & \sin\phi_i & 0 & 0 \\ -\sin\phi_i & \cos\phi_i & 0 & 0 \\ 0 & 0 & 1 & 0 \\ 0 & 0 & 0 & 1 \end{bmatrix}, \mathbf{R}_{\chi,i} = \begin{bmatrix} \cos\chi_i & 0 & \sin\chi_i & 0 \\ 0 & 1 & 0 & 0 \\ -\sin\chi_i & 0 & \cos\chi_i & 0 \\ 0 & 0 & 0 & 1 \end{bmatrix},$$

$$\mathbf{R}_{\varepsilon,i} = \begin{bmatrix} 1 & 0 & 0 & 0 \\ 0 & \cos\varepsilon_i & \sin\varepsilon_i & 0 \\ 0 & -\sin\varepsilon_i & \cos\varepsilon_i & 0 \\ 0 & 0 & 0 & 1 \end{bmatrix}.$$

The rotation matrix from UAV coordinate system to the geographic coordinate system:

$$\mathbf{R}_{U,i}^{G} = \mathbf{R}_{\kappa,i} \mathbf{R}_{\gamma,i} \mathbf{R}_{\eta,i}, \tag{A3}$$

$$\text{where } \mathbf{R}_{\kappa,i} = \begin{bmatrix} \cos\kappa_i & \sin\kappa_i & 0 & 0 \\ -\sin\kappa_i & \cos\kappa_i & 0 & 0 \\ 0 & 0 & 1 & 0 \\ 0 & 0 & 0 & 1 \end{bmatrix}, \mathbf{R}_{\gamma,i} = \begin{bmatrix} \cos\gamma_i & 0 & \sin\gamma_i & 0 \\ 0 & 1 & 0 & 0 \\ -\sin\gamma_i & 0 & \cos\gamma_i & 0 \\ 0 & 0 & 0 & 1 \end{bmatrix},$$

$$\mathbf{R}_{\eta,i} = \begin{bmatrix} 1 & 0 & 0 & 0 \\ 0 & \cos\eta_i & \sin\eta_i & 0 \\ 0 & -\sin\eta_i & \cos\eta_i & 0 \\ 0 & 0 & 0 & 1 \end{bmatrix}.$$

The rotation matrix of the geographic coordinate system to the ECEF coordinate system:

$$\mathbf{R}_{G,i}^{E} = \mathbf{R}_{M,i}\mathbf{R}_{L,i}, \tag{A4}$$

where $\mathbf{R}_{M,i} = \begin{bmatrix} \cos M_i & -\sin M_i & 0 & 0 \\ \sin M_i & \cos M_i & 0 & 0 \\ 0 & 0 & 1 & 0 \\ 0 & 0 & 0 & 1 \end{bmatrix}$, $\mathbf{R}_{L,i} = \begin{bmatrix} 1 & 0 & 0 & 0 \\ 0 & \cos L_i & \sin L_i & 0 \\ 0 & -\sin L_i & \cos L_i & 0 \\ 0 & 0 & 0 & 1 \end{bmatrix}$.

Appendix B. The Error of the Rotation Matrix Caused by the First-Order Noise of the Variable

The error sources of the rotation matrix between coordinate systems are different, and the error of the rotation matrix is represented by the noise of each parameter in the form of a full differential equation as follows: Express the error in the rotation matrix of the camera-to-base coordinate system in terms of the gimbal angle measurements:

$$\Delta\tilde{\mathbf{R}}_{C,i}^{B} = \mathrm{d}\tilde{\mathbf{R}}_{C,\alpha_i}^{B}\Delta\alpha_i + \mathrm{d}\tilde{\mathbf{R}}_{C,\beta_i}^{B}\Delta\beta_i = \tilde{\mathbf{R}}_r\tilde{\mathbf{R}}_{\alpha,i}\Delta\tilde{\mathbf{R}}_{\beta,i}\Delta\alpha_i + \tilde{\mathbf{R}}_r\Delta\tilde{\mathbf{R}}_{\alpha,i}\tilde{\mathbf{R}}_{\beta,i}\Delta\beta_i, \tag{A5}$$

where $\Delta\tilde{\mathbf{R}}_{\alpha,i} = \begin{bmatrix} \sin\tilde{\alpha}_i & \cos\tilde{\alpha}_i & 0 & 0 \\ -\cos\tilde{\alpha}_i & \sin\tilde{\alpha}_i & 0 & 0 \\ 0 & 0 & 1 & 0 \\ 0 & 0 & 0 & 1 \end{bmatrix}$, $\Delta\tilde{\mathbf{R}}_{\beta,i} = \begin{bmatrix} 1 & 0 & 0 & 0 \\ 0 & \sin\tilde{\beta}_i & -\cos\tilde{\beta}_i & 0 \\ 0 & \cos\tilde{\beta}_i & \sin\tilde{\beta}_i & 0 \\ 0 & 0 & 0 & 1 \end{bmatrix}$.

The error in the rotation matrix of the base-to-UAV coordinate system is expressed in terms of vibration angle measurements:

$$\begin{aligned} \Delta\tilde{\mathbf{R}}_{B,i}^{U} =& \mathrm{d}\tilde{\mathbf{R}}_{B,\phi_i}^{U}\Delta\phi_i + \mathrm{d}\tilde{\mathbf{R}}_{B,\chi_i}^{U}\Delta\chi_i + \mathrm{d}\tilde{\mathbf{R}}_{B,\varepsilon_i}^{U}\Delta\varepsilon_i \\ =& \Delta\tilde{\mathbf{R}}_{\phi,i}\tilde{\mathbf{R}}_{\chi,i}\tilde{\mathbf{R}}_{\varepsilon,i}\Delta\phi_i + \tilde{\mathbf{R}}_{\phi,i}\Delta\tilde{\mathbf{R}}_{\chi,i}\tilde{\mathbf{R}}_{\varepsilon,i}\Delta\chi_i + \tilde{\mathbf{R}}_{\phi,i}\tilde{\mathbf{R}}_{\chi,i}\Delta\tilde{\mathbf{R}}_{\varepsilon,i}\Delta\varepsilon_i, \end{aligned} \tag{A6}$$

where $\Delta\tilde{\mathbf{R}}_{\phi,i} = \begin{bmatrix} \sin\tilde{\phi}_i & -\cos\tilde{\phi}_i & 0 & 0 \\ \cos\tilde{\phi}_i & \sin\tilde{\phi}_i & 0 & 0 \\ 0 & 0 & 1 & 0 \\ 0 & 0 & 0 & 1 \end{bmatrix}$, $\Delta\tilde{\mathbf{R}}_{\chi,i} = \begin{bmatrix} \sin\tilde{\chi}_i & 0 & -\cos\tilde{\chi}_i & 0 \\ 0 & 1 & 0 & 0 \\ \cos\tilde{\chi}_i & 0 & \sin\tilde{\chi}_i & 0 \\ 0 & 0 & 0 & 1 \end{bmatrix}$,

$\Delta\tilde{\mathbf{R}}_{\varepsilon,i} = \begin{bmatrix} 1 & 0 & 0 & 0 \\ 0 & \sin\tilde{\varepsilon}_i & -\cos\tilde{\varepsilon}_i & 0 \\ 0 & \cos\tilde{\varepsilon}_i & \sin\tilde{\varepsilon}_i & 0 \\ 0 & 0 & 0 & 1 \end{bmatrix}$.

Use the attitude angle measurements of UAV to represent the error in the rotation matrix of the UAV-to-geographic coordinate system:

$$\begin{aligned} \Delta\tilde{\mathbf{R}}_{U,i}^{G} =& \mathrm{d}\tilde{\mathbf{R}}_{U,\kappa_i}^{G}\Delta\kappa_i + \mathrm{d}\tilde{\mathbf{R}}_{U,\gamma_i}^{G}\Delta\gamma_i + \mathrm{d}\tilde{\mathbf{R}}_{U,\eta_i}^{G}\Delta\eta_i \\ =& \Delta\tilde{\mathbf{R}}_{\kappa,i}\tilde{\mathbf{R}}_{\gamma,i}\tilde{\mathbf{R}}_{\eta,i}\Delta\kappa_i + \tilde{\mathbf{R}}_{\kappa,i}\Delta\tilde{\mathbf{R}}_{\gamma,i}\tilde{\mathbf{R}}_{\eta,i}\Delta\gamma_i + \tilde{\mathbf{R}}_{\kappa,i}\tilde{\mathbf{R}}_{\gamma,i}\Delta\tilde{\mathbf{R}}_{\eta,i}\Delta\eta_i, \end{aligned} \tag{A7}$$

where $\Delta\tilde{\mathbf{R}}_{\kappa,i} = \begin{bmatrix} \sin\tilde{\kappa}_i & -\cos\tilde{\kappa}_i & 0 & 0 \\ \cos\tilde{\kappa}_i & \sin\tilde{\kappa}_i & 0 & 0 \\ 0 & 0 & 1 & 0 \\ 0 & 0 & 0 & 1 \end{bmatrix}$, $\Delta\tilde{\mathbf{R}}_{\gamma,i} = \begin{bmatrix} \sin\tilde{\gamma}_i & 0 & -\cos\tilde{\gamma}_i & 0 \\ 0 & 1 & 0 & 0 \\ \cos\tilde{\gamma}_i & 0 & \sin\tilde{\gamma}_i & 0 \\ 0 & 0 & 0 & 1 \end{bmatrix}$,

$\Delta\tilde{\mathbf{R}}_{\eta,i} = \begin{bmatrix} 1 & 0 & 0 & 0 \\ 0 & \sin\tilde{\eta}_i & -\cos\tilde{\eta}_i & 0 \\ 0 & \cos\tilde{\eta}_i & \sin\tilde{\eta}_i & 0 \\ 0 & 0 & 0 & 1 \end{bmatrix}$.

Use the GPS measurements of UAV to represent the error in rotation matrix of the geographic-to-ECEF coordinate system:

$$\Delta\tilde{\mathbf{R}}^{E}_{G,i} = \mathrm{d}\tilde{\mathbf{R}}^{E}_{G,M_i}\Delta M_i + \mathrm{d}\tilde{\mathbf{R}}^{E}_{G,L_i}\Delta L_i = \Delta\tilde{\mathbf{R}}_{M,i}\tilde{\mathbf{R}}_{L,i}\Delta M_i + \tilde{\mathbf{R}}_{M,i}\Delta\tilde{\mathbf{R}}_{L,i}\Delta L_i, \tag{A8}$$

$$\text{where } \Delta\tilde{\mathbf{R}}_{M,i} = \begin{bmatrix} \sin\tilde{M}_i & \cos\tilde{M}_i & 0 & 0 \\ -\cos\tilde{M}_i & \sin\tilde{M}_i & 0 & 0 \\ 0 & 0 & 1 & 0 \\ 0 & 0 & 0 & 1 \end{bmatrix}, \Delta\tilde{\mathbf{R}}_{L,i} = \begin{bmatrix} 1 & 0 & 0 & 0 \\ 0 & \sin\tilde{L}_i & -\cos\tilde{L}_i & 0 \\ 0 & \cos\tilde{L}_i & \sin\tilde{L}_i & 0 \\ 0 & 0 & 0 & 1 \end{bmatrix}.$$

References

1. Zhao, S.; Zhang, X.P.; Cui, X.; Lu, M. A Closed-Form Localization Method Utilizing Pseudorange Measurements From Two Nonsynchronized Positioning Systems. *IEEE Internet Things J.* **2021**, *8*, 1082–1094. [CrossRef]
2. Kim, J.; Kim, J.Y.; Jeon, S.; Baik, J.W.; Cho, S.H.; Kim, C. Super-Resolution Localization Photoacoustic Microscopy Using Intrinsic Red Blood Cells as Contrast Absorbers. *Light Sci. Appl.* **2019**, *8*, 103. [CrossRef] [PubMed]
3. Heil, H.S.; Schreiber, B.; Götz, R.; Emmerling, M.; Dabauvalle, M.C.; Krohne, G.; Höfling, S.; Kamp, M.; Sauer, M.; Heinze, K.G. Sharpening Emitter Localization in Front of a Tuned Mirror. *Light Sci. Appl.* **2018**, *7*, 99. [CrossRef] [PubMed]
4. Wang, Y.; Ho, K.C. An Asymptotically Efficient Estimator in Closed-Form for 3-D AOA Localization Using a Sensor Network. *IEEE Trans. Wireless Commun.* **2015**, *14*, 6524–6535. [CrossRef]
5. Masullo, L.A.; Stefani, F.D. Multiphoton Single-Molecule Localization by Sequential Excitation with Light Minima. *Light Sci. Appl.* **2022**, *11*, 70. [CrossRef]
6. Masullo, L.A.; Szalai, A.M.; Lopez, L.F.; Pilo-Pais, M.; Acuna, G.P.; Stefani, F.D. An Alternative to MINFLUX That Enables Nanometer Resolution in a Confocal Microscope. *Light Sci. Appl.* **2022**, *11*, 199. [CrossRef]
7. Cao, S.; Chen, X.; Zhang, X.; Chen, X. Combined Weighted Method for TDOA-Based Localization. *IEEE Trans. Instrum. Meas.* **2020**, *69*, 1962–1971. [CrossRef]
8. Shen, H.; Ding, Z.; Dasgupta, S.; Zhao, C. Multiple source localization in wireless sensor networks based on time of arrival measurement. *IEEE Trans. Signal Process.* **2014**, *62*, 1938–1949. [CrossRef]
9. Park, P.; Marco, P.D.; Jung, M.; Santucci, F.; Sung, T.K. Multidirectional Differential RSS Technique for Indoor Vehicle Navigation. *IEEE Internet Things J.* **2023**, *10*, 241–253. [CrossRef]
10. Dogancay, K. Bias Compensation for the Bearings-Only Pseudolinear Target Track Estimator. *IEEE Trans. Signal Process.* **2006**, *54*, 59–68. [CrossRef]
11. Kang, X.; Wang, D.; Shao, Y.; Ma, M.; Zhang, T. An Efficient Hybrid Multi-Station TDOA and Single-Station AOA Localization Method. *IEEE Trans. Wireless Commun.* **2023**, *22*, 5657–5670. [CrossRef]
12. Sun, S.; Zhang, X.; Zheng, C.; Fu, J.; Zhao, C. Underwater Acoustical Localization of the Black Box Utilizing Single Autonomous Underwater Vehicle Based on the Second-Order Time Difference of Arrival. *IEEE J. Ocean. Eng.* **2020**, *45*, 1268–1279. [CrossRef]
13. Kim, T.y.; Hwang, S.s. Cascade AOA Estimation Algorithm Based on Flexible Massive Antenna Array. *Sensors* **2020**, *20*, 6797. [CrossRef] [PubMed]
14. Bai, G.; Liu, J.; Song, Y.; Zuo, Y. Two-UAV Intersection Localization System Based on the Airborne Optoelectronic Platform. *Sensors* **2017**, *17*, 98. [CrossRef]
15. Rui, L.; Ho, K. Bias Analysis of Maximum Likelihood Target Location Estimator. *IEEE Trans. Aerosp. Electron. Syst.* **2014**, *50*, 2679–2693. [CrossRef]
16. Wang, Y.; Ho, K.C. Unified Near-Field and Far-Field Localization for AOA and Hybrid AOA-TDOA Positionings. *IEEE Trans. Wireless Commun.* **2018**, *17*, 1242–1254. [CrossRef]
17. Chen, X.; Wang, G.; Ho, K. Semidefinite Relaxation Method for Unified Near-Field and Far-Field Localization by AOA. *Signal Process.* **2021**, *181*, 107916. [CrossRef]
18. Sun, Y.; Ho, K.C.; Wan, Q. Eigenspace Solution for AOA Localization in Modified Polar Representation. *IEEE Trans. Signal Process.* **2020**, *68*, 2256–2271. [CrossRef]
19. Sadeghi, M.; Behnia, F.; Amiri, R. Optimal Sensor Placement for 2-D Range-Only Target Localization in Constrained Sensor Geometry. *IEEE Trans. Signal Process.* **2020**, *68*, 2316–2327. [CrossRef]
20. Doğançay, K.; Hmam, H. Optimal Angular Sensor Separation for AOA Localization. *Signal Process.* **2008**, *88*, 1248–1260. [CrossRef]
21. Fang, X.; Li, J.; Zhang, S.; Chen, W.; He, Z. Optimal AOA Sensor-Source Geometry With Deployment Region Constraints. *IEEE Commun. Lett.* **2022**, *26*, 793–797. [CrossRef]
22. Xu, S.; Dogancay, K. Optimal Sensor Placement for 3-D Angle-of-Arrival Target Localization. *IEEE Trans. Aerosp. Electron. Syst.* **2017**, *53*, 1196–1211. [CrossRef]
23. Smith, W.H.F. Direct Conversion of Latitude and Height from One Ellipsoid to Another. *J. Geod.* **2022**, *96*, 36. [CrossRef]
24. Kay, S.M. *Fundamentals of Statistical Signal Processing: Estimation Theory*; Prentice-Hall, Inc.: Upper Saddle River, NJ, USA , 1993.
25. Golub, G.H.; Van Loan, C.F. *Matrix Computations*; JHU Press: Baltimore, MD, USA, 2013.

26. Wang, Y.; Ho, K.C. TDOA Positioning Irrespective of Source Range. *IEEE Trans. Signal Process.* **2017**, *65*, 1447–1460. [CrossRef]
27. Moreno-Salinas, D.; Pascoal, A.; Aranda, J. Optimal sensor placement for acoustic underwater target positioning with range-only measurements. *IEEE J. Ocean. Eng.* **2016**, *41*, 620–643. [CrossRef]
28. Zhang, Y.; Ho, K. Multistatic localization in the absence of transmitter position. *IEEE Trans. Signal Process.* **2019**, *67*, 4745–4760. [CrossRef]